Condensin II plays an essential role in reversible assembly of mitotic chromosomes in situ

Takao Ono[a], Chiyomi Sakamoto[b], Mitsuyoshi Nakao[b], Noriko Saitoh[b,†], and Tatsuya Hirano[a,*]
[a]Chromosome Dynamics Laboratory, RIKEN, 2-1 Hirosawa, Wako, Saitama 351-0198, Japan; [b]Department of Medical Cell Biology, Institute of Molecular Embryology and Genetics, Kumamoto University, 2-2-1 Honjo, Chuo-ku, Kumamoto 860-0811, Japan

ABSTRACT **Condensins I and II are multisubunit complexes that play a central role in mitotic chromosome assembly. Although both complexes become concentrated along the axial region of each chromatid by metaphase, it remains unclear exactly how such axes might assemble and contribute to chromosome shaping. To address these questions from a physicochemical point of view, we have established a set of two-step protocols for inducing reversible assembly of chromosome structure in situ, namely within a whole cell. In this assay, mitotic chromosomes are first expanded in a hypotonic buffer containing a Mg^{2+}-chelating agent and then converted into different shapes in a NaCl concentration-dependent manner. Both chromatin and condensin-positive chromosome axes are converted into near-original shapes at 100 mM NaCl. This assay combined with small interfering RNA depletion demonstrates that the recovery of chromatin shapes and the reorganization of axes are highly sensitive to depletion of condensin II but less sensitive to depletion of condensin I or topoisomerase IIα. Furthermore, quantitative morphological analyses using the machine-learning algorithm wndchrm support the notion that chromosome shaping is tightly coupled to the reorganization of condensin II-based axes. We propose that condensin II makes a primary contribution to mitotic chromosome architecture and maintenance in human cells.**

Monitoring Editor
Orna Cohen-Fix
National Institutes of Health

Received: Apr 20, 2017
Revised: Aug 15, 2017
Accepted: Aug 16, 2017

INTRODUCTION

When eukaryotic cells divide, chromatin residing within the interphase nucleus is converted into a discrete set of individual chromosomes, each composed of a pair of rod-shaped chromatids (sister chromatids). This process, known as mitotic chromosome assembly or condensation, is an essential prerequisite for faithful segregation of genetic information into two daughter cells. Despite enormous progress marked during the past two decades or so, its molecular mechanism remains not fully understood (Belmont, 2006; Marko, 2008; Kinoshita and Hirano, 2017).

It is generally thought that the protein composition of mitotic chromosomes is highly complex, especially because they represent one of the largest structures observed within the cell. In fact, a recent proteomics approach has identified ~4000 proteins in mitotic chromosomes isolated from chicken DT40 cells (Ohta *et al.*, 2010). It should be noted, however, that this number includes domain-specific components (e.g., centromere- and telomere-specific proteins) and contaminants that may artificially get associated with chromosomes during their isolation. It is therefore possible that the "core" components required for building the bulk part of mitotic chromosomes is much simpler, as had been shown in classical studies of metaphase chromosomes isolated from HeLa cells (Gasser and Laemmli, 1987) or mitotic chromatids assembled in *Xenopus* egg cell-free extracts (Hirano and Mitchison, 1994). In fact, only two factors, topoisomerase IIα (topo IIα) and condensin I, have been demonstrated so far to be essential for mitotic chromatid assembly in the cell-free extracts (Hirano and Mitchison, 1993; Hirano *et al.*, 1997). Equally important, a recent study has demonstrated that mitotic chromosome-like structures can be reconstituted in vitro by

This article was published online ahead of print in MBoC in Press (http://www.molbiolcell.org/cgi/doi/10.1091/mbc.E17-04-0252) on August 23, 2017.

†Present address: Cancer Institute of the Japanese Foundation for Cancer Research, 3-8-31 Ariake, Koto-ku, Tokyo 135-8550, Japan.

*Address correspondence to: Tatsuya Hirano (hiranot@riken.jp).

Abbreviations used: H3K9me3, histone H3 trimethylated at Lys-9; IMS, intrinsic metaphase structure; PFA, paraformaldehyde; PI, propidium iodide; SCC, sodium chloride-induced chromosome conversion; SMC, structural maintenance of chromosomes; topo IIα, topoisomerase IIα; wndchrm, weighted neighbor distances using a compound hierarchy of algorithms representing morphology.

mixing sperm chromatin with only six purified components, which include core histones, topo IIα, and condensin I (Shintomi *et al.*, 2015). Moreover, once assembly reactions are complete, removing topo IIα from mitotic chromosomes has little impact on their morphology in the *Xenopus* egg cell-free extracts (Hirano and Mitchison, 1993). A recent study has used the same cell-free extracts to demonstrate that chromosome-like structures can be assembled even in the near absence of nucleosomes (Shintomi *et al.*, 2017). Taken together with other cell biological and genetic studies during the past several years, it seems fair to conclude that condensins are the most important, central players in the assembly and structural maintenance of mitotic chromosomes (Thadani *et al.*, 2012; Frosi and Haering, 2015; Hirano, 2016; Kalitsis *et al.*, 2017).

Most eukaryotic cells have two different condensin complexes, known as condensins I and II, each composed of five subunits (Thadani *et al.*, 2012; Frosi and Haering, 2015; Hirano, 2016). Whereas the two condensin complexes share the same pair of structural maintenance of chromosomes (SMC) ATPase subunits (SMC2/CAP-E and SMC4/CAP-C), they are characterized by distinct sets of nonSMC regulatory subunits: CAP-D2, -G, and -H in condensin I and CAP-D3, -G2, and -H2 in condensin II. This difference in subunit composition confers their differential distributions and actions during the cell cycle (Hirota *et al.*, 2004; Ono *et al.*, 2004; Gerlich *et al.*, 2006). For instance, condensin I is sequestered into the cytoplasm from interphase through prophase and gains access to chromosomes only after the nuclear envelope breaks down in prometaphase. In contrast, condensin II is predominantly nuclear throughout interphase and contributes to early stages of chromosome assembly in prophase. By metaphase, both condensin complexes become concentrated along the central axial region of each chromatid where condensin II is more internal to condensin I (Ono *et al.*, 2003). It remains unclear, however, exactly how the condensin-positive axes might assemble and to what extent the axial structure contributes to the overall morphology of chromosomes (Belmont, 2006; Marko, 2008; Hirano, 2016).

It is well known that the morphology of mitotic chromosomes is highly sensitive to buffer conditions to which they are exposed (Cole, 1967; Earnshaw and Laemmli, 1983; Poirier and Marko, 2002). Moreover, the observations that mitotic chromosome structures can reversibly be expanded and recompacted under certain experimental conditions have attracted cell biologists' attention for a long time. For example, a pioneering study by Cole (1967) reported that alternate treatments of isolated chromosomes with Mg^{2+}-chelating and Mg^{2+}-containing buffers cause swelling (expansion) and shrinking (recovery), respectively, and that such a cycle of morphological changes can be repeated multiple times. More recently, Hudson *et al.* (2003) applied a similar assay, which they called the intrinsic metaphase structure (IMS) assay, to whole cells, demonstrating that the reversible recovery of chromosome morphology depends on SMC2, a core subunit common to both condensins I and II. We reasoned that such manipulation of chromosome morphology may be useful for further probing physico-chemical property of the condensin-based axes and its contribution to chromosome shaping.

In the current study, we have modified and extended the previously described protocols for reversible assembly of mitotic chromosome structures in situ, namely within a whole cell cultured on a coverslip. We first developed a two-step protocol for probing chromatin shapes and the condensin-positive axes, in which Na^+ is used instead of Mg^{2+} for reversible manipulation of chromosome structures ("sodium chloride-induced chromosome conversion [SCC] assay"). We then combined small interfering RNA (siRNA)-mediated depletion with the SCC assay to address the relative contribution of condensins I and II to these processes. Our results showed that the recovery of chromatin shapes and the reorganization of chromosome axes were both sensitive to depletion of condensin II but less sensitive to depletion of condensin I or topo IIα. To further validate our conclusions, we used a supervised machine-learning algorithm, weighted neighbor distances using a compound hierarchy of algorithms representing morphology (wndchrm) (Orlov *et al.*, 2008). Taken all together, our current results shed light on the differential contribution of condensins I and II to mitotic chromosome architecture and maintenance.

RESULTS

Morphological changes of chromatin and condensin-positive axes exposed to different buffer conditions

In the original protocol described by Hudson *et al.* (2003), chicken DT40 cells were exposed to TEEN buffer (1 mM triethanolamine-HCl [pH 8.5], 0.2 mM EDTA, and 25 mM NaCl) to expand mitotic chromosomes in situ. We first examined the impact of each ingredient of TEEN on the morphology of chromatin and chromosome axes. To this end, mitotic HeLa cells cultured on coverslips were exposed to TEEN, TEN (1 mM triethanolamine-HCl [pH 8.5] and 25 mM NaCl), or N (25 mM NaCl), and fixed with 2% paraformaldehyde (PFA) dissolved in the same solutions used for the treatment. As a control, a fraction of the mitotic cells was directly fixed without any treatment. These cells were immunolabeled with antibodies against SMC2 and topoisomerase IIα (topo IIα), and stained with 4′, 6-diamidino-2-phenylindole (DAPI). In the current study, "chromatin" was defined as DAPI-positive structures, whereas "axes" was defined as intrachromosomal structures positive for condensin labeling. Although chromatin displayed a compact appearance in a rosette-like configuration before treatment (Figure 1A, before), it largely expanded and displayed a cloudlike appearance in cells exposed to TEEN (Figure 1A, TEEN), in accordance with the observation reported by Hudson *et al.* (2003). In the expanded chromatin, SMC2-positive axes swelled and displayed a diffuse morphology. The signals of topo IIα dispersed even more broadly than those of SMC2. In the TEN-treated and N-treated cells, morphological changes of chromatin and axes were much milder than those observed in the TEEN-treated cells (Figure 1A, TEN and N), indicating that 0.2 mM EDTA included in TEEN has a very big impact on the morphological perturbation of chromatin and axes under this condition, which we call "step 1."

We then immersed the TEEN-treated cells in a $MgCl_2$-containing buffer, RSB (10 mM Tris-HCl [pH 7.4], 10 mM NaCl, and 5 mM $MgCl_2$), and fixed them in RSB. Although the expanded chromatin returned to a highly compact shape at this "step 2," as described by Hudson *et al.* (2003), we noticed that signals of SMC2 and topo IIα were hardly detectable in the recovered chromatin by immunofluorescence (Figure 1B, 2% PFA in RSB). Intriguingly, when the RSB-treated cells were fixed in phosphate-buffered saline (PBS; 10 mM Na_2HPO_4, 1.8 mM KH_2PO_4 [pH 7.5], 137 mM NaCl, and 2.7 mM KCl), signals of SMC2 and topo IIα became detectable (Figure 1B, 2% PFA in PBS). The shape of chromatin fixed in PBS was, however, much fuzzier, than that fixed in RSB, indicating that the morphology and antibody accessibility of chromosomes alters even during the fixation step depending on buffer conditions (additional evidence for the negative impact of Mg^{2+} on the antibody accessibility is shown in Supplemental Figure S1).

This notion further prompted us to test to what extent the fixation condition would affect the morphology of chromosomes in an experiment when 25 mM NaCl was used instead of RSB at step 2. Again, we found that 2% PFA in 25 mM NaCl and 2% PFA in PBS produced strikingly different morphology of both chromatin and

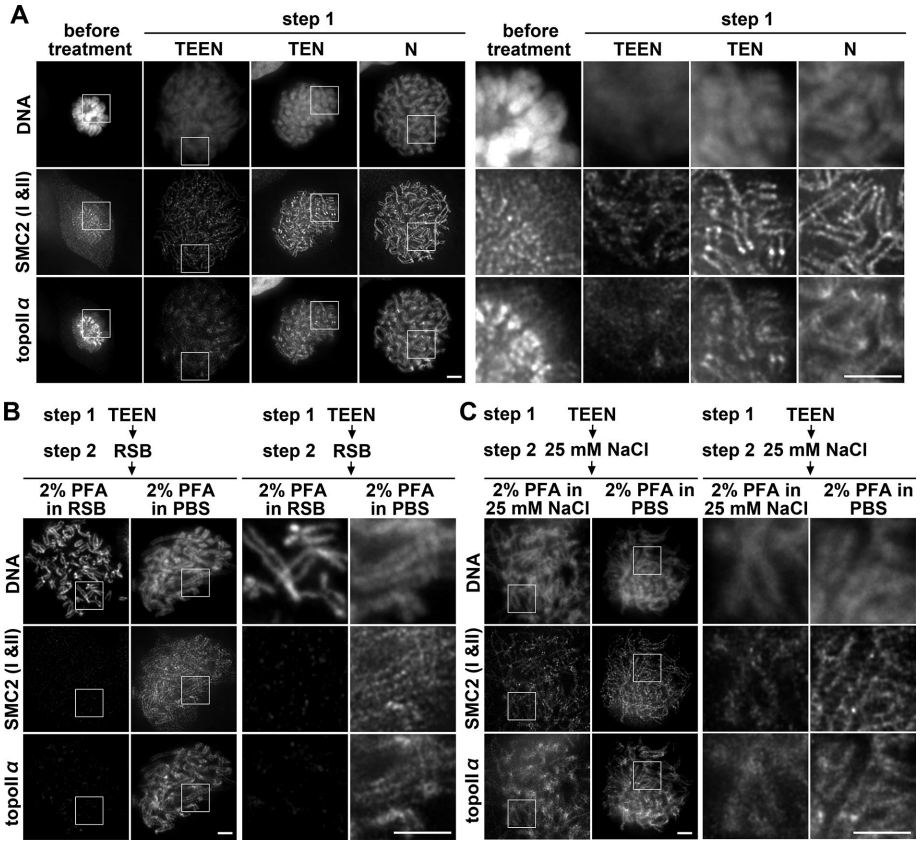

FIGURE 1: Morphological changes of chromatin and condensin-positive axes of cells exposed to different buffer conditions. (A) After colcemid treatment for 3 h, HeLa cells grown on coverslips were directly fixed with 2% PFA in PBS buffer (before treatment). Alternatively, cells were exposed to different buffers at step 1: TEEN (1 mM triethanolamine-HCl [pH 8.5], 0.2 mM EDTA, and 25 mM NaCl), TEN (1 mM triethanolamine-HCl [pH 8.5] and 25 mM NaCl), or N (25 mM NaCl). After the treatments at room temperature for 15 min, the cells were fixed with 2% PFA in the same buffers as those used for step 1 and then permeabilized with 0.5% Triton X-100 in PBS. The cells were subjected to immunolabeling with antibodies against SMC2 and topo IIα and stained with DAPI. Shown here are representative images of more than 11 captured under each of the four different conditions (left panels), along with blowups of the areas indicated by the white rectangles (right panels). Bar, 5 μm. (B) After the treatment with TEEN at step 1, the cells were exposed to RSB buffer (10 mM Tris-HCl [pH 7.4], 10 mM NaCl, and 5 mM $MgCl_2$) at step 2 for 15 min. The cells were then fixed with 2% PFA in RSB or in PBS buffer. After permeabilization, the cells were processed for immunolabeling and DAPI staining, as described in A. Shown here are representative images of more than 12 under each of the two fixation conditions (left panels), along with blowups of the areas indicated by the white rectangles (right panels). Bar, 5 μm. (C) In a different set of experiments, cells treated with TEEN at step 1 were exposed to 25 mM NaCl and then fixed with 2% PFA in 25 mM NaCl or with 2% PFA in PBS. Shown here are representative images of more than 6 captured under each of the two fixation conditions (left panels), along with blowups of the areas indicated by the white rectangles (right panels). Bar, 5 μm.

axes (Figure 1C). Thus we keenly realized that an extra care should be taken especially when the salt concentrations substantially differ between the fixation solutions and the treatment solutions used immediately before fixation. On the basis of these observations, we used PFA dissolved in the same buffer as the one used for the final treatment throughout the experiments reported below.

Establishment of the sodium chloride-induced chromosome conversion assay

To ensure subsequent immunolabeling of condensins and topo IIα, we sought to set up an alternative protocol that utilized solutions containing no Mg^{2+} at step 2. To this end, TEEN-treated cells at step 1 were exposed to solutions containing different concentrations of NaCl at step 2. We observed remarkable and highly reproducible morphological changes of chromatin and axes in a manner dependent on NaCl concentrations (Figure 2A). Although a treatment with 25 mM NaCl induced only subtle changes (Figure 2A, 25 mM NaCl), a treatment with 100 mM NaCl effectively returned the TEEN-treated chromatin into its near-original shape with a clearly discernible pair of rod-shaped chromatids (Figure 2A, 100 mM NaCl). Under this condition, both SMC2 and topo IIα displayed continuous, axial localization along each chromatid although the topo IIα signals originally enriched at the centromere regions was not restored. When 150 mM NaCl was used at step 2, chromatids became thinner and closer to each other (Figure 2A, 150 mM NaCl). Likewise, SMC2-positive axes displayed a thinner and more continuous appearance under this condition. Finally, a treatment with 300 mM NaCl at step 2 converted the expanded chromatin into multiple masses with a characteristic "ball-shaped" appearance (Figure 2A, 300 mM NaCl). The size and number of the balls observed were variable among different cells. Although no rod-shaped, individual chromosomes were observed, irregular axislike structures positive for SMC2 were observed within the chromatin masses. Intriguingly, topo IIα no longer colocalized with SMC2, apparently being displaced from chromatin under this condition.

To further validate the assay described above, we performed a semiquantitative analysis to classify the chromatin morphology observed (Figure 2B; see the figure legend for details). When the three different solutions (TEEN, TEN, and N) were used at step 1 (Figure 1A), we found that TEEN is most potent to perturb the shape of chromatin (Figure 2C). Classification of the morphology of chromatin observed at step 2 showed a very clear dependence of the extent of chromatin recovery on the NaCl concentration used (Figure 2D). Thus, by modifying the IMS assay originally described by Hudson *et al.* (2003), we established a new set of protocols for assessing the ability of chromosomes to reversibly restore their morphology in a NaCl concentration-dependent manner. Unlike the IMS assay, our assay enables us to follow the reorganization of condensin-positive axes at step 2 by immunofluorescence (Figure 2A). Hereafter we call this assay the "sodium chloride-induced chromosome conversion" (SCC) assay. Among the conditions tested, 100 mM NaCl was most efficient to recover chromatin shape and reorganize chromosome axes into their original appearances (Figure 2E; additional characterization of the SCC assay is shown in Supplemental Figure S2).

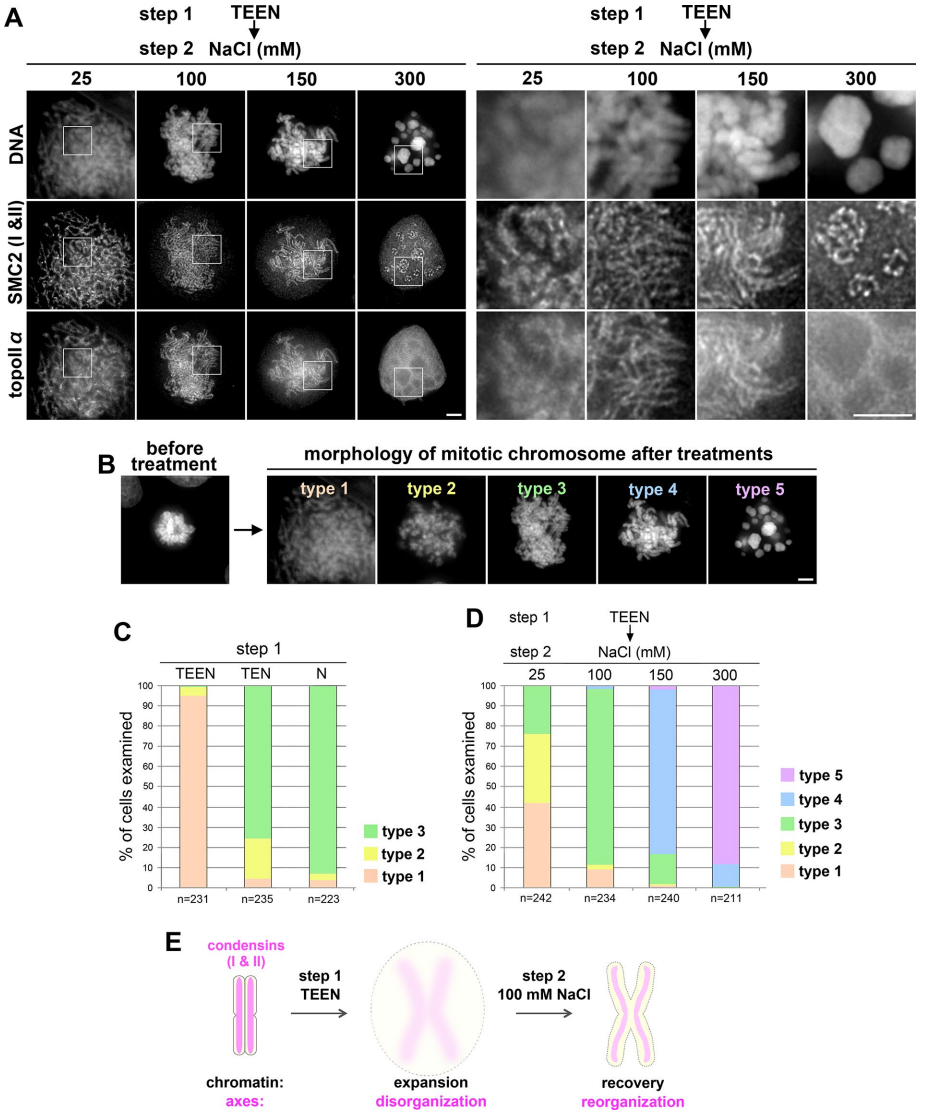

FIGURE 2: Recovery of the chromatin shape and reorganization of the axis structure using NaCl. (A) After being treated with TEEN at step 1, cells were exposed to different concentrations of NaCl as indicated at room temperature for 15 min (step 2). The cells were fixed with 2% PFA in the solutions containing the same NaCl concentrations used at step 2. After permeabilization, the cells were immunolabeled with anti-SMC2 and anti-topo IIα and stained with DAPI. Shown here are representative images of 22 images captured under each condition from two repeated experiments (left panels), along with blowups of the areas indicated by the white rectangles (right panels). Bar, 5 μm. (B) The morphologies of mitotic chromosomes observed at step 1 and step 2 were classified into five categories: type 1, severely expanded mass of chromatin with barely recognizable individual chromosomes (from A, 25 mM NaCl); type 2, expanded mass of chromatin with partially recognizable individual chromosomes; type 3, individual chromosomes with discernible sister chromatids that are close to the original appearance of chromosomes (from A, 100 mM NaCl); type 4, individual chromosomes with thin and kinky appearance of chromatids (from A, 150 mM NaCl); and type 5, discrete "ball"-like masses of chromatin (from A, 300 mM NaCl). (C) Plotted here are the frequencies of morphology observed under the three different conditions at step 1 shown in Figure 1A. The data shown are from a single representative experiment out of three repeats. (D) Plotted here are the frequencies of morphology observed under the four different conditions at step 2 shown in A. The data shown are from a single representative experiment out of three repeats. (E) Summary of the SCC assay described in Figure 1 and here. When mitotic cells are exposed to TEEN containing EDTA at step 1, chromatin largely expands ("expansion"). Condensin-positive axes are disorganized, displaying widely diffuse appearance ("disorganization"). When the cells are then treated with 100 mM NaCl, expanded chromatin is recompacted ("recovery"), and disorganized axes are restored ("reorganization"), thereby exhibiting near-original shapes.

Behaviors of condensins I and II and other nonaxial chromosomal markers in the SCC assay

We next examined other structural features of chromosomes observed at each step (before treatment, TEEN at step 1, and 100 or 300 mM NaCl at step 2) in the SCC assay using several different markers (Figure 3, A–C; Supplemental Figure S3, A–C). We first examined the distribution of condensins I and II. Cells before treatment showed that signals of both condensins I and II are differentially concentrated to the axial regions along the chromatids (Figure 3A, before). After treatment with TEEN at step 1, both signals became diffuse, although some signs of their distribution on discontinuous axial structures were discernible (Figure 3A, step 1). When cells were exposed to 100 mM NaCl at step 2, each signal of condensins I and II returned to the central region of rod-shaped chromatids (Figure 3A, step 2). Intriguingly, when 300 mM NaCl was used at step 2, condensins I and II displayed strikingly different localizations. Although condensin II signals were detected as irregular structures within the ball-shaped chromatin mass, most signals of condensin I were no longer confined to them (Supplemental Figure S3A), indicating that the irregular axislike structures labeled with anti-SMC2 (Figure 2A) are primarily composed of condensin II.

To probe the response of centromeres during the SCC assay, we then used anti-CENP-A and anti-centromere antibody-(ACA) positive antiserum, the latter of which recognizes CENP-A, -B, and -C (Muro *et al.*, 1990). We found that, on TEEN treatment at step 1, each CENP-A signal remained compact, but the distance between sister CENP-A signals largely increased (Figure 3B, before and step 1). At step 2 with 100 mM NaCl, the distance between sister CENP-A signals returned to the distance before treatment (Figure 3B, step 2). We also tested histone H3 trimethylated at Lys-9 (H3K9me3), a marker for pericentromeric heterochromatin (Guenatri *et al.*, 2004; Sullivan and Karpen, 2004). At step1 with TEEN, H3K9me3-positive areas vastly expanded up to approximately four-fold compared with those observed in cells before treatment (Figure 3C, before and step 1). At step 2 with 100 mM NaCl, the H3K9me3-positive regions shrunk again to a near-original level (Figure 3C, step 2). At step 2 with 300 mM NaCl, multiple pairs of CENP-A signals and multiple areas positive for H3K9me3 were observed within each of the ball-shaped chromatin masses (Supplemental Figure S3, B and C), suggesting that

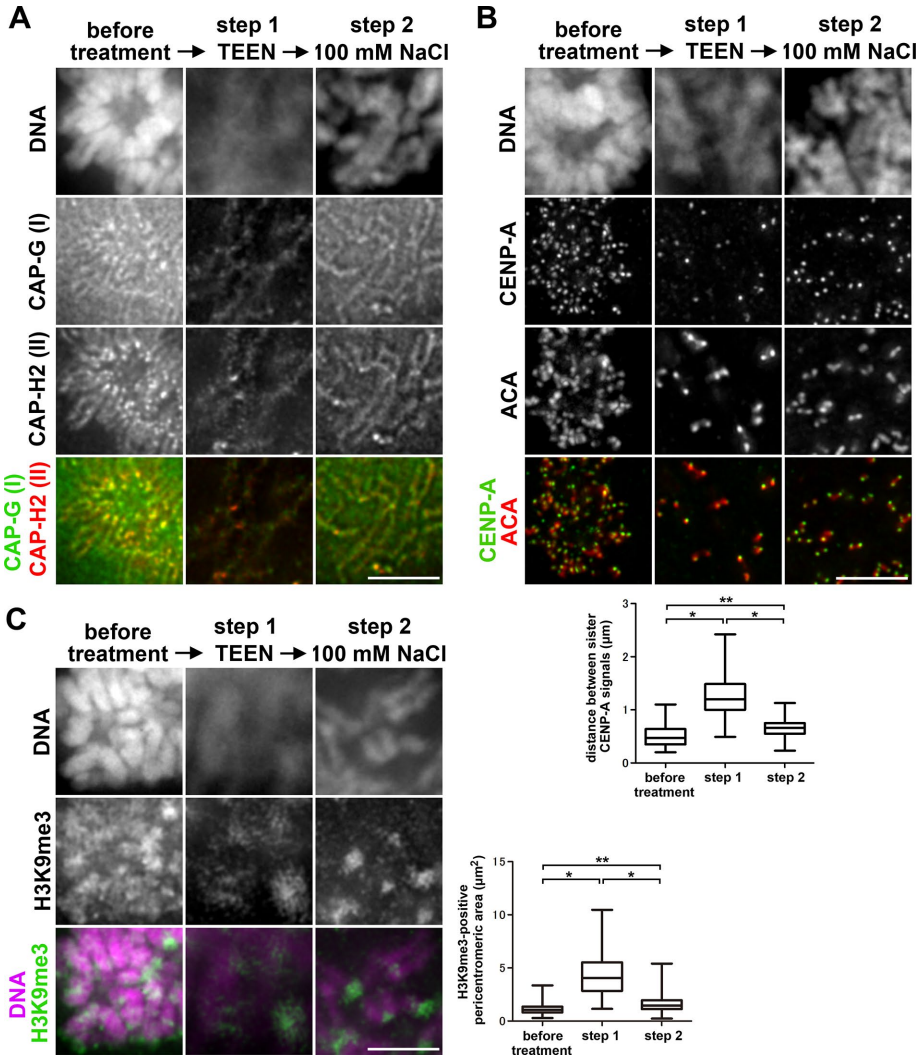

FIGURE 3: Localization of axial and nonaxial chromosomal markers in the SCC assay. After colcemid treatment for 3 h, HeLa cells grown on coverslips were directly fixed with 2% PFA in PBS (before treatment) and then treated with TEEN (step 1) or treated with TEEN (step1) and then with 100 mM NaCl (step 2). The cells were fixed in 2% PFA in the corresponding buffers, followed by permeabilization with 0.5% Triton X-100 in PBS. (A) Cells were immunolabeled with antibodies against a condensin I-specific subunit (CAP-G) and a condensin II-specific subunit (CAP-H2) and then stained with DAPI. Representative images at each step are shown. Shown here are representative images of more than 17 captured at each step from two repeated experiments. Bar, 5 μm. (B) Cells were immunolabeled with anti–CENP-A and ACA-positive antiserum and then stained with DAPI. Bar, 5 μm. Plots of measured distance between sister CENP-A signals are shown at the bottom. Under each condition, >253 pairs of sister CENP-A signals (>6 cells) were analyzed. Values of median, average, and SD in each step are as follows (μm): 0.47, 0.5, and 0.19 before treatment; 1.2, 1.26, and 0.37 at step 1; 0.66, 0.65, and 0.16 at step 2. The single asterisks (*) indicate statistically significant differences ($p < 0.01$), and the double asterisks (**) indicate no significant differences ($p < 0.1$) by Dunn's multiple comparison tests. The assessment was completed once. Bar, 5 μm. (C) Cells were immunolabeled with anti-H3K9me3 and stained with DAPI. Bar, 5 μm. Plots of measured areas of H3K9me3-positive pericentromeric regions are shown at the right. Under each condition, >232 areas (>9 cells) were analyzed. Values of median, average, and SD in each step are as follows (μm^2): 1.06, 1.14, and 0.47 before treatment; 4.06, 4.28, and 1.86 at step 1; 1.45, 1.57, and 0.67 at step 2. The single asterisks (*) indicate statistically significant differences ($p < 0.01$), and the double asterisks (**) indicate no significant differences ($p < 0.1$) by Dunn's multiple comparison tests. The assessment was completed once.

that each mass is composed of multiple chromosomes rather than a single chromosome.

Taken all together, these results showed that not only bulk chromatin but also pericentromeric chromatin are recovered to a near-original shape under the standard protocol, and suggest that histone modifications, at least as judged by H3K9me3, are largely preserved throughout these recovery processes.

Contribution of condensins to chromatin recovery and axis reorganization

We then wished to test which protein components constituting chromosome axes (condensin I, condensin II, and topo IIα) might make a primary contribution to their reorganization in the current assay and how depletion of each one of them might affect the behavior of the other components. In the first set of experiments, we prepared cells depleted of SMC2, condensin I-specific subunit (CAP-G), or condensin II-specific subunit (CAP-G2) by using specific siRNAs (the validation of depletion is shown in Supplemental Figure S4, A–D). The set of depleted cells was subjected to the standard SCC assay (i.e., TEEN at step 1 and 100 mM NaCl at step 2) and immunolabeled with antibodies against SMC2 and topo IIα. Although mock-depleted cells showed a proper recovery in their chromatin shape, cells depleted of SMC2 displayed a very fuzzy appearance of the chromatin at step 2 (Figure 4, A and B, siRNA, mock, and SMC2). In the SMC2-depleted cells, topo IIα displayed diffuse distribution and was no longer enriched at axial regions. Furthermore, we observed a better recovery of chromatin morphology in CAP-G-depleted cells than in CAP-G2-depeted cells (Figure 4, A and B, siRNA, CAP-G, and CAP-G2). Although the remaining SMC2 signals looked similar between the two sets of cells, topo IIα nicely restored its axial localization in the cells depleted of CAP-G but of CAP-G2. These results suggested that the axial localization of topo IIα depends more on condensin II than on condensin I and that condensin II plays a more crucial role in the proper recovery of chromatin structure than condensin I does. We also applied the Mg^{2+}-based IMS assay to HeLa cells and obtained the same conclusion (Supplemental Figure S4F).

In the second set of experiments, we examined the effect of topo IIα depletion (for the validation of depletion, see Supplemental Figure S4, A and E). Mock-depleted and topo IIα-depleted cells were subjected to the standard SCC assay and immunolabeled with antibodies against SMC2 and topo IIα. We found that the recovery of chromatin shapes and the reorganization of axes occurred normally (Figure 4C, siRNA, topo IIα), indicating that, unlike condensin II, topo IIα does not have a big contribution to these

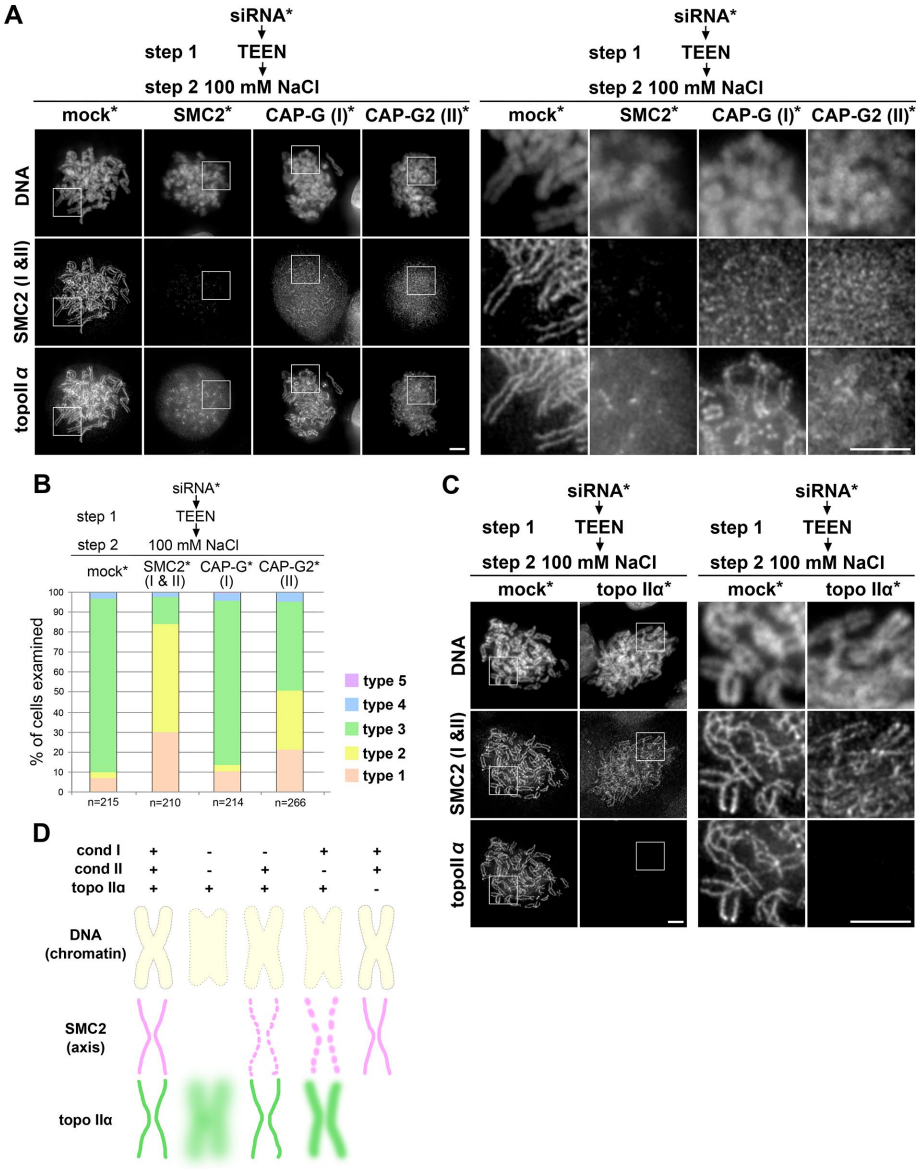

FIGURE 4: Contribution of condensins to chromatin recovery and axis reorganization. (A) Asynchronous HeLa cell cultures were transfected with a control siRNA (mock) and siRNAs specific to the condensin subunits indicated. After treatment with colcemid, the cells were first exposed to TEEN (step 1) and then to 100 mM NaCl (step 2). They were fixed and immunolabeled with anti-SMC2 and anti–topo IIα and stained with DAPI. Shown here are representative images (left panels), along with blowups of the areas indicated by the white rectangles (right panels). Bar, 5 μm. (B) Plotted here are the frequencies of morphology observed in cells mock-depleted and depleted of condensins at step 2 shown in A. The classification of chromatin shapes are shown in Figure 2B. The data shown are from a single representative experiment of three repeats. (C) HeLa cells were transfected with a control siRNA and an siRNA specific to topo IIα, subjected to the SCC assay, and processed as in A. Shown here are representative images of more than 27 captured under each condition from two repeated experiments. Bar, 5 μm. (D) Summary of the observations shown here (see the text).

processes. A summary of our observations in the SCC assay using cells depleted of condensins and topo IIα is shown in Figure 4D.

Analyses of chromosome morphology using a machine-learning algorithm

In general, it is not easy to collect precise quantitative information on chromosome morphology. This is because specimens are a mixture of many chromosomes with different lengths: identifying specific chromosomes from the mixture requires technically demanding assays such as in situ hybridization. It is also difficult to evaluate a cellular status representing a heterogeneous population (e.g., Figure 2, C and D) and properly quantitate various textures of chromosomes, such as the smoothness/fuzziness of the chromatin surface and/or the rigidity/irregularity of the chromosome axes. To overcome these problems and to further validate the conclusion described above, we sought to introduce a supervised machine-learning algorithm, wndchrm, into our analyses: This algorithm had been developed for automated image classification and mining of image similarities or differences (Orlov *et al.*, 2008) and was recently applied to several objectives, including cellular shapes and nuclear morphology (Tokunaga *et al.*, 2014; Kitamura *et al.*, 2015).

We repeated the same set of experiments as that shown in Figure 4A, and DAPI-stained images were acquired at each step (before treatment, step 1 with TEEN, and step 2 with 100 mM NaCl). Fifty images from each depleted group were randomly divided into two subgroups and processed for wndchrm analyses in parallel (galleries of images used for these analyses are shown in Supplemental Figure S5). In each step, the phylogeny of morphological distance (MD) among depleted cells (left) and the degrees of MD relative to one of the mock-depleted group (siCont_1) (right) are shown (Figure 5, A–C).

In the phylogeny for the condition of direct fixation (before treatment), the two subgroups derived from each depleted group were closely clustered with each other, and they were distantly branched from those derived from the other depleted groups, thereby nicely validating the competence of this classification method (Figure 5A, left). When compared with control cells, larger values of MD were detected in cells depleted of SMC2 and CAP-G2, but lower values were obtained with cells depleted of CAP-G, suggesting that morphological defect by depletion of condensin I was relatively small as judged by this method.

At step 1 with TEEN, the phylogeny showed that differences in the MD values among differently depleted groups became small, suggesting that the expansion with TEEN canceled the original differences in chromatin morphology created by depletion of condensin subunits (Figure 5B). In fact, the Pearson correlation coefficient of the phylogenies between Figure 5, A and B, was very small ($r = 0.475$).

At step 2 with 100 mM NaCl, the MD values of SMC2-depleted and CAP-G2-depleted groups relative to mock-depleted ones became remarkably large (Figure 5C). In contrast, the MD values of

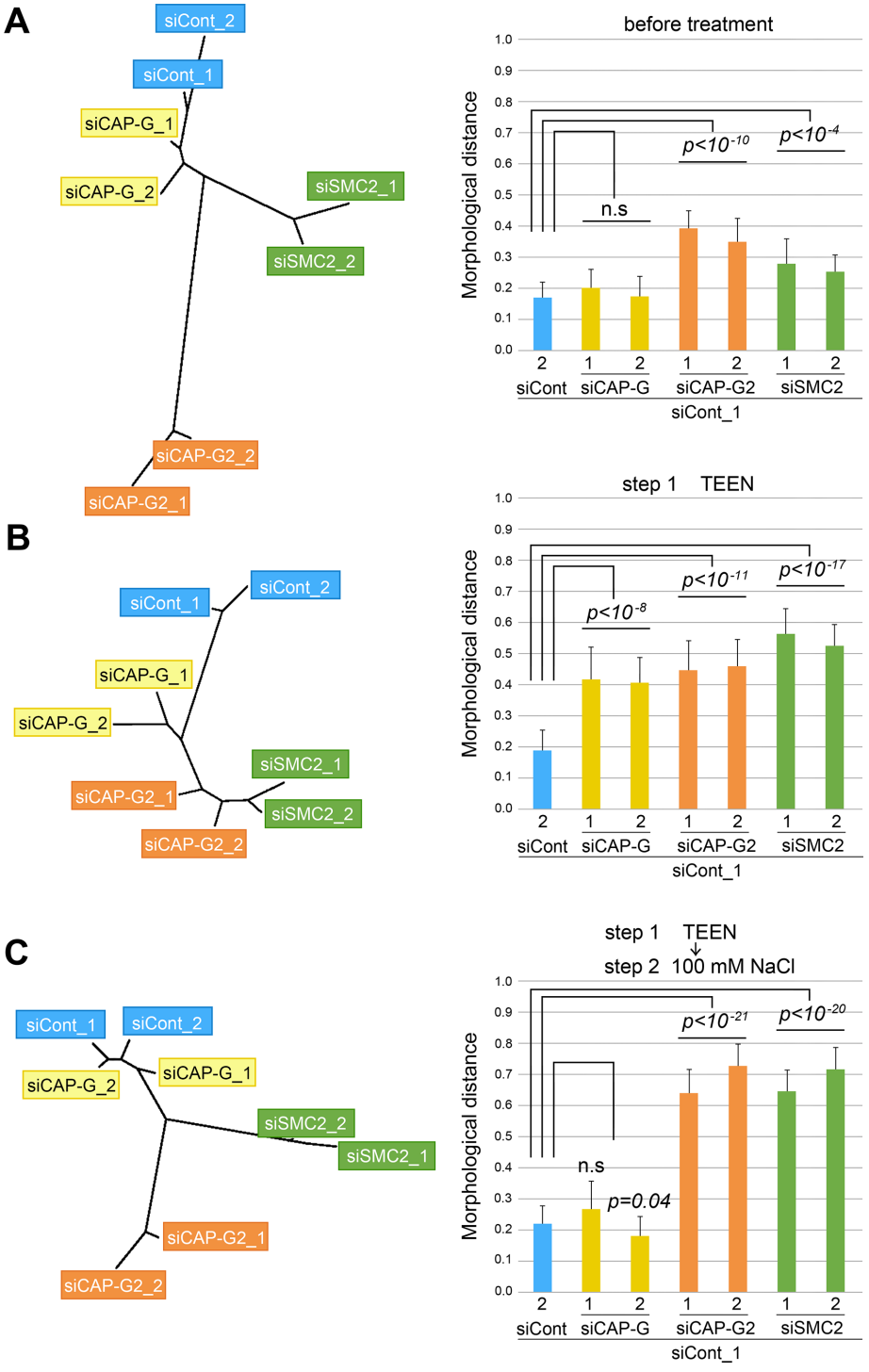

FIGURE 5: Quantitative analyses of morphological change of chromatin in the SCC assay. (A–C) HeLa cells mock-depleted (siCont) and depleted of condensins (siCAP-G, siCAP-G2, and siSMC2) were prepared as described in Figure 4A. After colcemid treatment, a fraction of cells was fixed directly and stained with DAPI (before treatment; A). Alternatively, the remaining cells were exposed to TEEN (step 1; B) or exposed to TEEN and then to 100 mM NaCl (step 2; C) and processed in the same way. Assessment of classification accuracy (CA) using different numbers of training images of siCont and siSMC2 cells before treatment (A) is shown in Supplemental Figure S7. The image similarities were computed with a supervised machine-learning algorithm (wndchrm) (see *Materials and Methods* for details). The phylogenies of DAPI-stained chromatin under each condition are shown on the left. The top 50 image features that were effective for classification are listed in Supplemental Table S1. Pearson correlation coefficients between the phylogenies were as follows: A and B, r = 0.475; A and C, r = 0.850; B and C, r = 0.578. The degrees of morphological changes from control cells (siCont_1) were computed as morphological distances (MDs) and plotted on the right. A large value of the MD indicates that the morphology differs from that of siCont_1 cells, such as ones of SMC2 depletions (siSMC2_1 and siSMC2_2; MD = 0.280 and 0.256, respectively, in A). siCont_2 served as a negative control with no morphological change from siCont_1 and showed small value (MD = 0.169 in A), as expected. Note that values of MD reflect branch lengths in phylogenies and are allowed to compare within the same condition. The values are means ± SE of 20 cross-validation tests.

CAP-G-depleted groups were very close to that of mock-depleted ones. Notably, the morphological differences between SMC2-depleted/CAP-G2-depleted groups and mock-depleted/CAP-G-depleted groups became more obvious at step 2 compared with "before treatment" (Figure 5A), although their relative positions were similar to each other. In fact, the Pearson correlation coefficient of the phylogenies between Figure 5, A and C, was high (r = 0.850). Thus the wndchrm analyses validated our previous conclusion that condensin II plays a more crucial role than condensin I in proper recovery of chromatin shapes in our SCC assay. Equally important, these results also demonstrate that the SCC assay is powerful in uncovering the architectural role of condensin II that would otherwise be less obvious in assays involving direct fixation of cells.

Wndchrm analyses support a tight coupling between condensin II-based axis reorganization and chromosome shaping

Next we examined the relationship between the recovery of chromatin shape and the reorganization of condensin-positive axes using the wndchrm analyses. In this round of experiments, topo IIα depletion was included as an additional control. We prepared the same set of siRNA-treated cells as that shown in Figure 4, A and C, and the cells were subjected to the standard SCC assay. They were then fixed and immunolabeled with anti-SMC2 and anti-topo IIα. We reasoned that SMC2 signals observed in cells depleted of CAP-G represent condensin II, whereas SMC2 signals observed in cells depleted of CAP-G2 represent condensin I. Images of chromatin shapes (DAPI), SMC2-positive axes, and topo IIα-positive axes were divided into two folders (Supplemental Figure S6) and then processed for wndchrm analyses as described above.

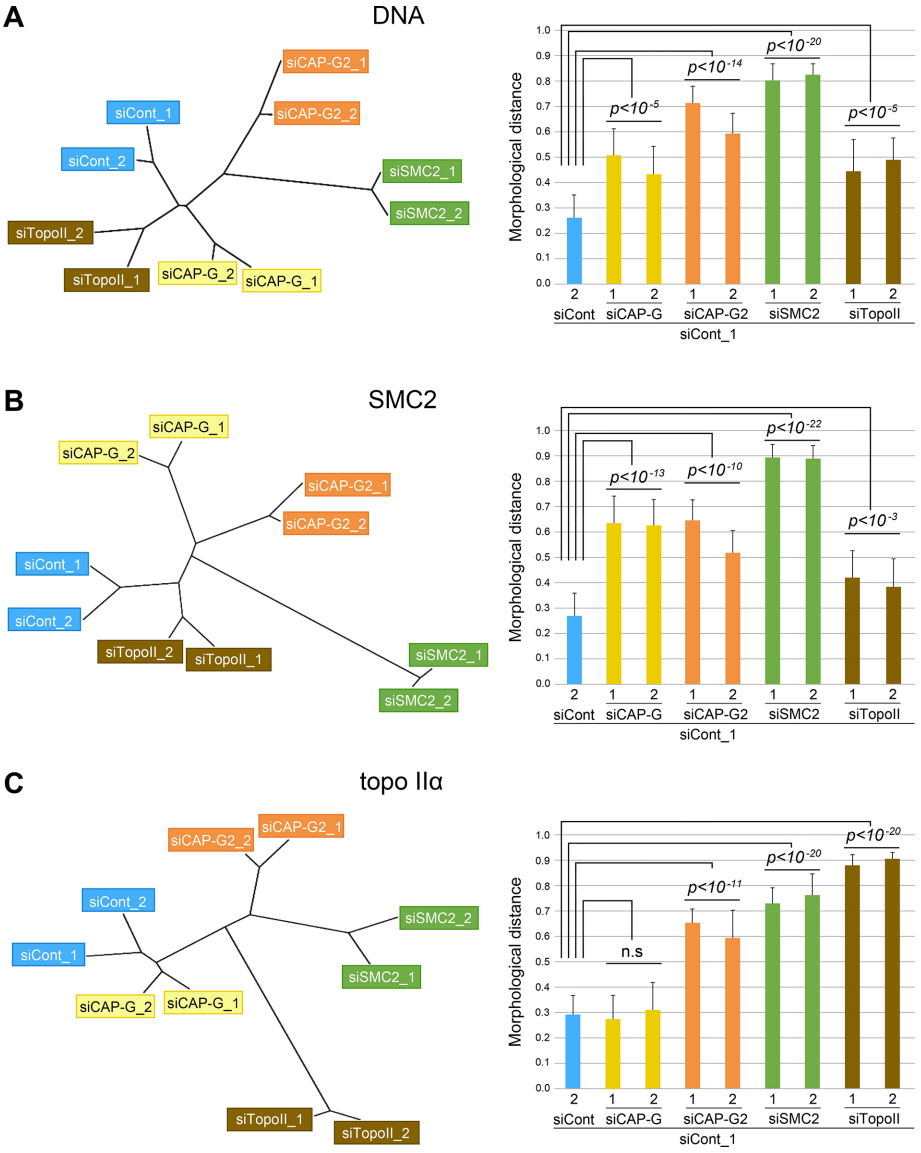

FIGURE 6: Quantitative analyses of chromatin recovery and axis reorganization. (A–C) HeLa cells mock (siCont) depleted, depleted of condensins (siCAP-G, siCAP-G2, and siSMC2), and depleted of topo IIα (siTopoII) were prepared described as in Figure 4, A and C. After treatment with colcemid, the cells were exposed to TEEN (step 1) and then to 100 mM NaCl (step 2). After fixation, the cells were stained with DAPI (A) and immunolabeled with anit-SMC2 (B) and anti–topo IIα (C). The images were subjected to the wndchrm analysis as described in Figure 5. The phylogenies are shown on the left. The top 50 image features that were effective for classification are listed in Supplemental Table S2. Pearson correlation coefficients between the phylogenies were as follows: A and B, r = 0.903; A and C, r = 0.821; B and C, r = 0.750. The MDs from siCont_1 are shown on the right. The values are means ± SE of 20 cross-validation tests.

Consistent with the data shown in Figure 5C, wndchrm analyses judged that most significant alterations in the shape of chromatin occurred in cells depleted of CAP-G2 and SMC2 (Figure 6A). Much less and equal levels of alterations were evaluated in cells depleted of CAP-G and topo IIα. Immunolabeled images with anti-SMC2 were then subjected to wndchrm analyses. Because SMC2 signals were barely detectable in cells depleted of SMC2, this group of cells were most distantly branched from any other groups in the phylogeny as expected (Figure 6B). Cells depleted of CAP-G and those depleted of CAP-G2 were modestly clustered, displaying equal distances from control cells. Notably, this wndchrm analysis judged that depletion of topo IIα had little impact on the morphology of SMC2-positive structures. The Pearson correlation coefficient of the phylogenies between chromatin shape (Figure 6A) and SMC2-positive axes (Figure 6B) was very high (r = 0.903), suggesting that there is a strong correlation between the recovery of chromatin shapes and the reorganization of condensin-based axes. We noticed, however, that there is a substantial difference between Figure 6, A and B, in the relative contribution of condensins I and II to the recovery of chromatin shapes. This implies that proper recovery of chromatin shapes is related more closely with the reorganization of condensin II-based axes than condensin I-based structures.

Finally, immunolabeled images with anti-topo IIα were subjected to wndchrm analyses. As expected, cells depleted of topo IIα were most distantly branched from the other groups in the phylogeny (Figure 6C). The MD values in cells depleted of CAP-G2 and depleted of SMC2 were quite high, and their relationship was modestly close to each other in the phylogeny. In fact, these two groups of cells displayed a very fuzzy signal of topo IIα (Figure 4A). In striking contrast, cells depleted of CAP-G were closely clustered with control cells. These results suggest that the axial enrichment of topo IIα observed in the SCC assay depends largely on condensin II but to lesser extent on condensin I.

DISCUSSION

It has been established that condensins I and II have central roles in mitotic chromosome assembly (Kschonsak and Haering, 2015; Hirano, 2016). It remains poorly understood, however, how chromosome axes might assemble, and to what extent the axial structure contributes to chromosome shaping. In the current study, we have devised a modified assay for probing salt-dependent, reversible assembly of mitotic chromosomes in situ and revealed the primary importance of condensin II-based axes in chromosome shaping. Also, the current study is arguably the first to apply a machine-learning algorithm to the evaluation of chromosome morphology and to the assessment of potential coupling between condensin-based axis formation and chromosome shaping.

A modified assay for probing reversible assembly of mitotic chromosomes in situ

Cation concentration-dependent, morphological changes had been reported at various levels of chromosome structure, including nucleosomal arrays to bulk chromatin masses (Hansen, 2002; Marko, 2008; Maeshima *et al.*, 2014; Pepenella *et al.*, 2014; Phengchat *et al.*, 2016). These observations were explained by the fact that negative charges of DNA, which are not fully neutralized by

positively charged histones, are shielded by cations, thereby allowing compaction of the DNA-containing structures. Similarly, the conversion of higher-order chromatin shapes also exploits the electrostatic properties of chromatin itself. When Mg^{2+} ions around chromatin are chelated with EDTA present in TEEN (step 1), negatively charged DNAs repel each other, displaying an expanded appearance of chromatin. When TEEN is replaced with RSB containing a high concentration (5 mM) of Mg^{2+} (step 2), the expanded chromatin gets recompacted, restoring a near-original shape of chromosomes in chicken DT40 cells (Hudson *et al.*, 2003). This high concentration of Mg^{2+} has since been used widely in the field (Hudson *et al.*, 2003; Spence *et al.*, 2007; Green *et al.*, 2012; Samejima *et al.*, 2012; Poonperm *et al.*, 2015). We noticed that, when the same protocol is applied to whole HeLa cells, mitotic chromosomes are converted into an unusually skinny appearance that failed to be immunolabeled with antibodies against SMC2 or topo IIα (Figure 1B, 2% PFA in RSB), raising the concern that chromatin may be excessively compacted to a nonphysiological level, as pointed out previously (Poirier and Marko, 2002).

In the current study, we therefore used various concentrations of NaCl at step 2 and found that chromosomes display highly reproducible recovery of their shapes in a NaCl concentration-dependent manner. Chromosomes properly reassemble with 100 mM NaCl in our protocol, and the resulting structures can readily be immunolabeled with antibodies against chromosomal proteins distributed axially or nonaxially. Although it is not completely understood how monovalent and divalent cations cooperatively create the ionic atmosphere around chromatin, their effects are not in accordance with the simple sum of their charge valencies and concentrations (Gan and Schlick, 2010). It remains an open question exactly how the ion atmosphere affects the conformation of DNA and chromosomal proteins including condensins I and II (also see below).

Successful immunolabeling in the SCC assay enabled us to analyze morphological changes of chromatin in greater detail. Based on immunofluorescence of H3K9me3 and CENP-A, both pericentromeric chromatin and inner centromeric chromatin undergo morphological changes along with bulk chromatin in the SCC assay (Figure 3, B and C). However, the dotlike appearance of CENP-A signals is resistant to TEEN treatment (Figure 3B), suggesting that CENP-A-containing centromeric chromatin has properties that differ from those of other parts of chromosomes, as was suggested before through the IMS assay using DT40 cells (Ribeiro *et al.*, 2009).

We noticed that, in parallel with the morphological changes of chromatin, axial distribution of condensins reappear at step 2 in a NaCl concentration-dependent manner (Figure 2A). Interestingly, although SMC2 signals display linear axial localization in a range of NaCl concentrations from 25 to 150 mM at step 2, they form irregular axislike structures in ball-shaped chromatin masses in 300 mM NaCl at step 2. Under the latter condition, topo IIα signals are no longer detectable on chromatin. In addition, whereas siRNA deletion of SMC2 compromises restoration of topo IIα axial localization, depletion of topo IIα has little impact on the reorganization of condensin-positive axes (Figure 4, A and C). These results strongly suggest that the reassembly of condensin-positive axes in the SCC assay occurs independently of topo IIα.

Relative contribution of condensins I and II to reversible assembly of mitotic chromosomes

Most eukaryotic species have two different condensin complexes. It appears that the relative contribution of condensins I and II to the assembly and structural maintenance of chromosomes varies among species and cell types. For instance, the abundance and function of condensin I are predominant over those of condensin II in *Xenopus* egg cell-free extracts (Ono *et al.*, 2003; Shintomi and Hirano, 2011). In contrast, condensin II plays a more important role than condensin I in keeping the rigidity of meiosis I chromosomes in mouse oocytes (Houlard *et al.*, 2015).

Our current results show that condensin II makes a primary contribution to the proper recovery of chromosome shapes in the SCC assay using HeLa cells (Figure 4A). As judged by the IMS assay using chicken DT40 cells, Green *et al.* (2012) reached the conclusion that condensin I has a slightly bigger contribution than condensin II to the recovery of chromosomes. The apparent discrepancy between the two studies could be explained by the use of different cell types (HeLa and chicken DT40 cells) rather than the use of different assays (the SCC and IMS assays). Consistent with this view, when the IMS assay was applied to HeLa cells, we obtained a result similar to that obtained with the SCC assay (Supplemental Figure S4F). One possible explanation is that the relative ratio of condensin I to II differs between the two cell types: Condensin I is more abundant than condensin II in DT40 cells (Ohta *et al.*, 2010; Green *et al.*, 2012), whereas the two complexes are equally abundant in HeLa cells (Ono *et al.*, 2003).

Our analyses using wndchrm validated the primary contribution of condensin II to proper recovery of chromatin (Figure 5) and supported the idea of a tight coupling between the condensin II-mediated reorganization of chromosome axes and chromosome shaping (Figure 6). Because of technical limitations inherently associated with the current assay, the possible contribution of condensin I to the reorganization process cannot be ruled out. It is nonetheless important to take several issues into consideration when one compares condensin I and condensin II. First, condensin II assembles axial structure in mitotic prophase before condensin I gains access to chromosomes in prometaphase (Ono *et al.*, 2003; Hirota *et al.*, 2004), and condensin II tends to be found more internally than condensin I in metaphase chromosomes (Figure 7, top). Second, a recent experiment using *Xenopus* egg cell-free extracts has shown that condensin II can assemble chromosome axes largely independently of nucleosomes, whereas condensin I's proper action depends on nucleosomes (Shintomi *et al.*, 2017). Third, condensin I is more dynamically exchange on metaphase chromosomes than condensin II, as judged by fluorescence recovery after photobleaching experiments (Gerlich *et al.*, 2006). It is most likely that the different pairs of HEAT (Huntingtin, elongation factor 3, the A subunit of protein phosphatase 2A and the signaling kinase TOR1) subunits present in the two condensin complexes contribute to their different behaviors in vivo and to their different NaCl-dependent responses in the SCC assay (Figure 7, inset). In fact, a recent in vitro assay using *Xenopus* egg extracts demonstrated that balancing act of the two HEAT subunits (CAP-D2 and CAP-G) of condensin I is required for dynamic assembly of chromosome axes (Kinoshita *et al.*, 2015). It is tempting to speculate that unique properties of amphipathic helices, structural elements constituting the HEAT repeats, might help to facilitate condensin-condensin attractions to assemble chromosome axes in vivo (Yoshimura and Hirano, 2016) as well as to reorganize them in the SCC assay in vitro. The different behaviors of condensins I and II could attribute to different biochemical and structural properties of their HEAT subunits. Future experiments using recombinant complexes should be of great help to clarify such properties.

Implications and perspectives

The current study extends numerous previous studies that emphasized rather complex and perplexing properties of chromatin and chromosomes. One of the classical examples of such studies was

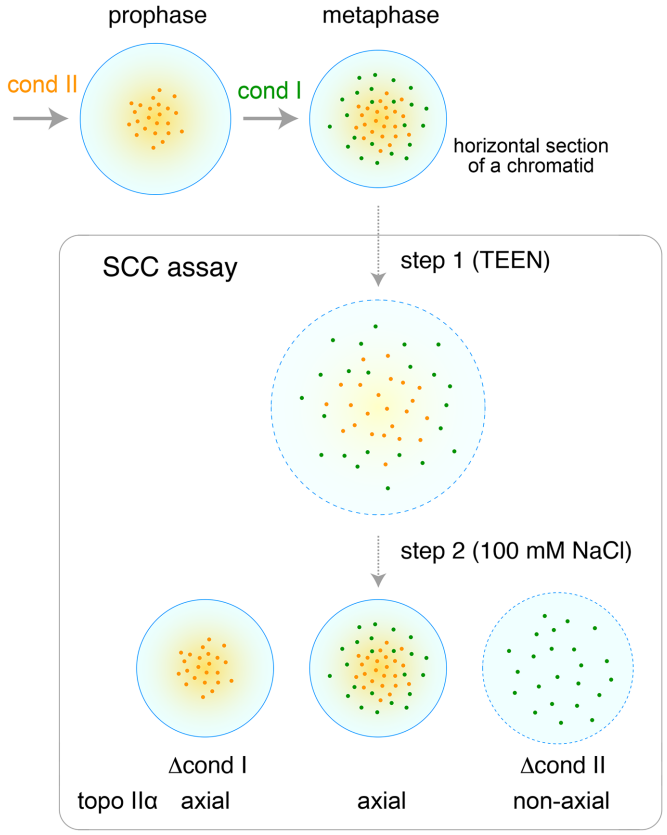

FIGURE 7: Model for differential behaviors of condensins I and II in the cell and in the SCC assays. In the cell, condensin II accumulates in the interior of chromatids by late prophase. After nuclear envelope breakdown in prometaphase, condensin I is recruited to and decorates the outside of the condensin II-based axes. In the SCC assay, axes once swollen at step 1 (TEEN) are reorganized into a near-original appearance at step 2 with the aid of condensins I and II (100 mM NaCl). Condensin II can properly reassemble its axial structure even in the absence of condensin I (Δcond II), whereas condensin I alone fails to do so, accompanying poorer recovery of chromatin shapes (Δcond I). In this cartoon, horizontal sections of chromatids are shown.

a preparation of the chromosome scaffold, a remnant, fibrous structure observed on depletion of histones from mitotic chromosomes in the presence of polyanion or high concentrations of salt (Paulson and Laemmli, 1977). Despite long debates about the physiological relevance of the chromosome scaffold, accumulating lines of evidence indicate that two major classes of proteins comprising the scaffold fraction indeed have essential functions in mitotic chromosome assembly (Earnshaw *et al.*, 1985; Saitoh *et al.*, 1994; Hirano *et al.*, 1997; Shintomi *et al.*, 2015; Shintomi *et al.*, 2017). In a sense, the current study represents part of the long-term effort that aims to understand classical observations of chromosome morphology with modern molecular terms. It is interesting to note that physico-chemical aspects of chromosomes are now being revisited, which include a liquidlike property of chromatin itself (Maeshima *et al.*, 2016; Larson *et al.*, 2017; Strom *et al.*, 2017) and charge-based repulsion between chromosome surfaces (Cuylen *et al.*, 2016). Given this situation, it will undoubtedly be important to further understand the physico-chemical properties of chromosome axes and the mechanistic contribution of condensins to building such structures. We believe that our SCC assay and related methods for manipulating chromosome structure will be useful in addressing these old and new questions in chromosome biology.

MATERIALS AND METHODS

Cell culture

HeLa cells used in the present study were provided from the RIKEN BioResource Center (Cell number, RCB0007), and maintained in a modified Eagle's medium (Sigma-Aldrich) supplemented with 10% FBS (SAFC Biosciences; Cat. No. 171012; Lot No. 7G0031) at 37°C in an atmosphere of 5% CO_2. For microscopic analyses, cells were grown on poly-L-lysine–coated coverslips as described previously (Ono *et al.*, 2004). Colcemid was added at a final concentration of 0.02 μg/ml to the culture medium, and incubation was continued for 3 h to enrich mitotic cells. After removal of the medium, the cells were subjected to various treatments in the same culture dishes.

siRNAs treatment

Stealth siRNAs were used for depletion experiments (Invitrogen/Life Technologies Japan, Tokyo). The sequences of the sense strand of the siRNAs were as follows:

SMC2 (CAP-E)_78, 5′-CUUCAAUGCUAUCACUGGCUUAAAU-3′
CAP-G_309, 5′-CUUAAAGUCUCAUGAAGCAAACAGC-3′
CAP- G2_351, 5′-AGCCCUACUGGAAUGUGUUAUUAUA-3′
topo IIα_80, 5′-AAGACUGUCUGUUGAAAGAAUCUAU-3′

Asynchronous HeLa cells were transfected with Stealth siRNA duplexes at a final concentration of 33.3 nM using Lipofectamine RNAiMAX (Invitrogen/Life Technologies Japan, Tokyo) according to the manufacturer's instructions. In the case of depletion of condensin subunits, transfection was performed twice along with Stealth RNAi Negative Control Med GC duplex (33.3 nM) as a control. In the case of depletion of topo IIα, transfection was performed once along with Stealth RNAi Negative Control Lo GC duplex (33.3 nM) as a control.

SCC assay

At the first step (step 1), cells on the coverslips in a culture plate with 24 wells were immersed in 1.4 ml of a hypotonic buffer containing a Mg^{2+}-chelating agent, TEEN buffer (1 mM triethanolamine-HCl [pH 8.5], 0.2 mM EDTA•2Na, and 25 mM NaCl) (Hudson *et al.*, 2003), for 15 min at room temperature. For experiments in Figure 1, TEN (1 mM triethanolamine-HCl [pH 8.5] and 25 mM NaCl) and N (25 mM NaCl) were used as buffers in step 1. After removal of buffers in step 1, at the second step (step 2), cells were immersed in 1.4 ml of another hypotonic buffer containing Mg^{2+}, RSB buffer (10 mM Tris-HCl [pH 7.4], 10 mM NaCl, and 5 mM $MgCl_2$) (Hudson *et al.*, 2003) or buffers including NaCl with indicated concentrations (ranging from 0 to 300 mM) at room temperature for 15 min. To check the changes of cell membrane permeability, propidium iodide (PI) at a final concentration of 50 μg/ml was applied to the cells at each step of the SCC assay and visualized (Supplemental Figure S2, A and B). Alternatively, the TEEN-treated cells were exposed to 10 mM HEPES buffer (pH 7.4) containing different concentrations of NaCl at step 2 (Supplemental Figure S2, C and D). To reduce the influence of the previous solution at each step as much as possible, buffers were replaced 3 times or more by half with fresh one. After treatment, if there is no description, cells on coverslips were fixed in 2% PFA in buffers identical to those processed immediately before, for 15 min at room temperature. These processes were performed in the same culture plate. The fixed cells were permeabilized with 0.5% Triton

X-100 in PBS at room temperature for 5 min before being processed for immunolabeling.

Antibodies used for immunolabeling

Rabbit polyclonal antibodies used in the present study were anti-human SMC2 (CAP-E), anti-human CAP-G (Kimura *et al.*, 2001), anti-human CAP-G2, and anti-human CAP-H2 (Ono *et al.*, 2003). Antibodies were used at a final concentration of 1 µg/ml for both immunoblotting and immunofluorescence. To perform double immunolabeling of condensins I and II (Figure 2A and Supplemental Figure S3A), antibodies against CAP-G and CAP-H2 were labeled with Alexa Fluor 568 and Alexa Fluor 488, respectively, using the Alexa Fluor protein labeling kit (Molecular Probes/Life Technologies Japan, Tokyo). In this case, antibodies were used at a final concentration of 5 µg/ml for CAP-G and 10 µg/ml for CAP-H2. Mouse monoclonal antibody (mAb) against human CENP-A (Ando *et al.*, 2002) and ACA-positive antiserum (Muro *et al.*, 1990; also known as CREST serum) were used at 1:5 dilution and 1:2,500 dilution, respectively. The following primary antibodies were purchased from commercial sources and used at a final concentration of 1 µg/ml: anti-human topoisomerase IIα (clone 1C5; MBL, Nagoya, Japan) and anti-H3K9me3 (07-523; Upstate/EMD Millipore, Darmstadt, Germany). The following secondary antibodies for immunolabeling were purchased from Molecular Probes/Thermo Fisher Scientific (Waltham, MA): Alexa Fluor 568 or 633 goat anti–human immunoglobulin G (IgG), Alexa Fluor 488 or 568 goat anti–mouse IgG, and Alexa Fluor 488 or 568 donkey anti-rabbit IgG. After immunolabeling, the coverslips were stained with 2 µg/ml DAPI for 5 min and then mounted with Vectashield (Vector Laboratories, Burlingame, CA). The secondary antibodies used for immunoblotting (goat anti-rabbit and goat anti-mouse HRP-conjugated IgG) were purchased from Vector Laboratories.

Microscopy

Fluorescence images were acquired with a DeltaVision restoration microscope system (Applied Precision), consisting of an inverted microscope (IX71; Olympus, Tokyo) with an UPlanSApo 100 ×/1.40 NA oil-immersion objective lens (Olympus). The image stacks of whole cells and chromosome spreads were acquired with a Z-step size of 0.5 and 0.2 µm, respectively. They were subjected to constrained iterative (10 iterations) deconvolution (Chen *et al.*, 1996) and then projected with five to eight sections using the softWoRx software ver.6.5.1 (Applied Precision/GE Healthcare UK Ltd, Little Chalfont, England). On the projected images, the distance between sister CENP-A signals (Figure 3B) was measured as described previously (Ono *et al.*, 2013). Pericentromeric areas with H3K9me3-positive signals were defined as areas with four times higher brightness than the surrounding areas and measured using the softWoRx software (Figure 3C). Grayscale images were pseudocolored and merged using Photoshop (Adobe, San Jose, CA), and statistical analyses were performed using the GraphPad Prism ver.5.02 (GraphPad Software, La Jolla, CA).

Morphological quantification of chromatin and axes

For quantitative assessment of chromosome structures, a supervised machine-learning algorithm, wndchrm ver. 1.52 (Orlov *et al.*, 2008; Kitamura *et al.*, 2015), was applied to 50 projected images in each condition, which was defined as a class. Images stained with DAPI (chromatin) in the SCC assay were preexcised to be placed in the center of the area within one cell in 260 × 260 pixels (Supplemental Figure S5A, before treatment) and 512 × 512 pixels (step 1 and step 2, Supplemental Figure S5, B and C). Immunolabeled images in recovered chromatin (step 2) were also preexcised to be placed in the center of the area within one cell in 400 × 400 pixels (Supplemental Figure S6). All of the images in the defined class were applied to wndchrm, and morphological feature values were assigned by training a machine. Phylogenies were computed using the Fitch-Margoliash method implemented in the PHYLIP package ver.3.696, which is based on pairwise class similarity values reported by wndchrm ver 1.52 (Felsensein, 1989; Johnston *et al.*, 2008). For each analysis, cross-validation tests were automatically repeated for 20 times with 17 training/8 test image data set. The options used for the image analysis were a large feature set of 2919 (-l) and multiprocessors (-m). To measure pairwise class dissimilarity, morphological distances (MD) were calculated as the Euclidean distances ($d = \sqrt{\Sigma[A-B]^2}$) from the values in class probability matrix obtained from the cross-validations (Johnston *et al.*, 2008). To calculate *p* values, a two-sided *t* test was performed for each of comparisons. To optimize the classification capacity, we measured classification accuracy (CA) using different numbers of training data sets and found that the accuracy reached a plateau with more than 25 images (Supplemental Figure S7). Then each image in a class (50 images) was randomly assigned to two independent sets (folder 1 and folder 2, each containing 25 images) to confirm that images within the same class (condition) show negligible differences. They were expected to localize closely in phylogenies and to show low MD between them.

ACKNOWLEDGMENTS

We are grateful to the late K. Yoda for CENP-A antibody and Y. Muro for ACA-positive antisera. We also thank A. Matsuura for excellent technical assistance and members of the Hirano laboratory for critically reading the manuscript. This work was supported by the Japan Society for the Promotion of Science (JSPS) KAKENHI (16K07455 [T.O.], 25116009 and 16H04744 [N.S.], 15H04707 [M.N.], and 26251003 [T.H.]).

REFERENCES

Ando S, Yang H, Nozaki N, Okazaki T, Yoda K (2002). CENP-A, -B, and -C chromatin complex that contains the I-type alpha-satellite array constitutes the prekinetochore in HeLa cells. Mol Cell Biol 22, 2229–2241.

Belmont AS (2006). Mitotic chromosome structure and condensation. Curr Opin Cell Biol 18, 632–638.

Chen H, Hughes DD, Chan TA, Sedat JW, Agard DA (1996). IVE (Image Visualization Environment): a software platform for all three-dimensional microscopy applications. J Struct Biol 116, 56–60.

Cole A (1967). Chromosome structure. Theoret Biophys 1, 305–375.

Cuylen S, Blaukopf C, Politi AZ, Muller-Reichert T, Neumann B, Poser I, Ellenberg J, Hyman AA, Gerlich DW (2016). Ki-67 acts as a biological surfactant to disperse mitotic chromosomes. Nature 535, 308–312.

Earnshaw WC, Halligan B, Cooke CA, Heck MM, Liu LF (1985). Topoisomerase II is a structural component of mitotic chromosome scaffolds. J Cell Biol 100, 1706–1715.

Earnshaw WC, Laemmli UK (1983). Architecture of metaphase chromosomes and chromosome scaffolds. J Cell Biol 96, 84–93.

Felsensein J (1989). PHYLIP: phylogeny inference package (version 3.2). Cladistics 5, 164–166.

Frosi Y, Haering CH (2015). Control of chromosome interactions by condensin complexes. Curr Opin Cell Biol 34, 94–100.

Gan HH, Schlick T (2010). Chromatin ionic atmosphere analyzed by a mesoscale electrostatic approach. Biophys J 99, 2587–2596.

Gasser SM, Laemmli UK (1987). Improved methods for the isolation of individual and clustered mitotic chromosomes. Exp Cell Res 173, 85–98.

Gerlich D, Hirota T, Koch B, Peters JM, Ellenberg J (2006). Condensin I stabilizes chromosomes mechanically through a dynamic interaction in live cells. Curr Biol 16, 333–344.

Green LC, Kalitsis P, Chang TM, Cipetic M, Kim JH, Marshall O, Turnbull L, Whitchurch CB, Vagnarelli P, Samejima K, *et al.* (2012). Contrasting roles of condensin I and condensin II in mitotic chromosome formation. J Cell Sci 125, 1591–1604.

Guenatri M, Bailly D, Maison C, Almouzni G (2004). Mouse centric and pericentric satellite repeats form distinct functional heterochromatin. J Cell Biol 166, 493–505.
Hansen JC (2002). Conformational dynamics of the chromatin fiber in solution: determinants, mechanisms, and functions. Annu Rev Biophys Biomol Struct 31, 361–392.
Hirano T (2016). Condensin-based chromosome organization from bacteria to vertebrates. Cell 164, 847–857.
Hirano T, Kobayashi R, Hirano M (1997). Condensins, chromosome condensation protein complexes containing XCAP-C, XCAP-E and a Xenopus homolog of the Drosophila Barren protein. Cell 89, 511–521.
Hirano T, Mitchison TJ (1993). Topoisomerase II does not play a scaffolding role in the organization of mitotic chromosomes assembled in Xenopus egg extracts. J Cell Biol 120, 601–612.
Hirano T, Mitchison TJ (1994). A heterodimeric coiled-coil protein required for mitotic chromosome condensation in vitro. Cell 79, 449–458.
Hirota T, Gerlich D, Koch B, Ellenberg J, Peters JM (2004). Distinct functions of condensin I and II in mitotic chromosome assembly. J Cell Sci 117, 6435–6445.
Houlard M, Godwin J, Metson J, Lee J, Hirano T, Nasmyth K (2015). Condensin confers the longitudinal rigidity of chromosomes. Nat Cell Biol 17, 771–781.
Hudson DF, Vagnarelli P, Gassmann R, Earnshaw WC (2003). Condensin is required for nonhistone protein assembly and structural integrity of vertebrate mitotic chromosomes. Dev Cell 5, 323–336.
Johnston J, Iser WB, Chow DK, Goldberg IG, Wolkow CA (2008). Quantitative image analysis reveals distinct structural transitions during aging in Caenorhabditis elegans tissues. PLoS One 3, e2821.
Kalitsis P, Zhang T, Marshall KM, Nielsen CF, Hudson DF (2017). Condensin, master organizer of the genome. Chromosome Res 25, 61–76.
Kimura K, Cuvier O, Hirano T (2001). Chromosome condensation by a human condensin complex in Xenopus egg extracts. J Biol Chem 276, 5417–5420.
Kinoshita K, Hirano T (2017). Dynamic organization of mitotic chromosomes. Curr Opin Cell Biol 46, 46–53.
Kinoshita K, Kobayashi TJ, Hirano T (2015). Balancing acts of two HEAT subunits of condensin I support dynamic assembly of chromosome axes. Dev Cell 33, 94–106.
Kitamura H, Matsumori H, Kalendova A, Hozak P, Goldberg IG, Nakao M, Saitoh N, Harata M (2015). The actin family protein ARP6 contributes to the structure and the function of the nucleolus. Biochem Biophys Res Commun 464, 554–560.
Kschonsak M, Haering CH (2015). Shaping mitotic chromosomes: From classical concepts to molecular mechanisms. Bioessays 37, 755–766.
Larson AG, Elnatan D, Keenen MM, Trnka MJ, Johnston JB, Burlingame AL, Agard DA, Redding S, Narlikar GJ (2017). Liquid droplet formation by HP1alpha suggests a role for phase separation in heterochromatin. Nature 547, 236–240.
Maeshima K, Imai R, Tamura S, Nozaki T (2014). Chromatin as dynamic 10-nm fibers. Chromosoma 123, 225–237.
Maeshima K, Rogge R, Tamura S, Joti Y, Hikima T, Szerlong H, Krause C, Herman J, Seidel E, DeLuca J, *et al*. (2016). Nucleosomal arrays self-assemble into supramolecular globular structures lacking 30-nm fibers. EMBO J 35, 1115–1132.
Marko JF (2008). Micromechanical studies of mitotic chromosomes. Chromosome Res 16, 469–497.
Muro Y, Sugimoto K, Okazaki T, Ohashi M (1990). The heterogeneity of anticentromere antibodies in immunoblotting analysis. J Rheumatol 17, 1042–1047.
Ohta S, Bukowski-Wills JC, Sanchez-Pulido L, Alves Fde L, Wood L, Chen ZA, Platani M, Fischer L, Hudson DF, Ponting CP, *et al*. (2010). The protein composition of mitotic chromosomes determined using multiclassifier combinatorial proteomics. Cell 142, 810–821.
Ono T, Fang Y, Spector DL, Hirano T (2004). Spatial and temporal regulation of Condensins I and II in mitotic chromosome assembly in human cells. Mol Biol Cell 15, 3296–3308.
Ono T, Losada A, Hirano M, Myers MP, Neuwald AF, Hirano T (2003). Differential contributions of condensin I and condensin II to mitotic chromosome architecture in vertebrate cells. Cell 115, 109–121.
Ono T, Yamashita D, Hirano T (2013). Condensin II initiates sister chromatid resolution during S phase. J Cell Biol 200, 429–441.
Orlov N, Shamir L, Macura T, Johnston J, Eckley DM, Goldberg IG (2008). WND-CHARM: Multi-purpose image classification using compound image transforms. Pattern Recognit Lett 29, 1684–1693.
Paulson JR, Laemmli UK (1977). The structure of histone-depleted metaphase chromosomes. Cell 12, 817–828.
Pepenella S, Murphy KJ, Hayes JJ (2014). Intra- and inter-nucleosome interactions of the core histone tail domains in higher-order chromatin structure. Chromosoma 123, 3–13.
Phengchat R, Takata H, Morii K, Inada N, Murakoshi H, Uchiyama S, Fukui K (2016). Calcium ions function as a booster of chromosome condensation. Sci Rep 6, 38281.
Poirier MG, Marko JF (2002). Micromechanical studies of mitotic chromosomes. J Muscle Res Cell Motil 23, 409–431.
Poonperm R, Takata H, Hamano T, Matsuda A, Uchiyama S, Hiraoka Y, Fukui K (2015). Chromosome scaffold is a double-stranded assembly of scaffold proteins. Sci Rep 5, 11916.
Ribeiro SA, Gatlin JC, Dong Y, Joglekar A, Cameron L, Hudson DF, Farr CJ, McEwen BF, Salmon ED, Earnshaw WC, Vagnarelli P (2009). Condensin regulates the stiffness of vertebrate centromeres. Mol Biol Cell 20, 2371–2380.
Saitoh N, Goldberg IG, Wood ER, Earnshaw WC (1994). ScII: an abundant chromosome scaffold protein is a member of a family of putative ATPases with an unusual predicted tertiary structure. J Cell Biol 127, 303–318.
Samejima K, Samejima I, Vagnarelli P, Ogawa H, Vargiu G, Kelly DA, de Lima Alves F, Kerr A, Green LC, Hudson DF, *et al*. (2012). Mitotic chromosomes are compacted laterally by KIF4 and condensin and axially by topoisomerase IIalpha. J Cell Biol 199, 755–770.
Shintomi K, Hirano T (2011). The relative ratio of condensin I to II determines chromosome shapes. Genes Dev 25, 1464–1469.
Shintomi K, Inoue F, Watanabe H, Ohsumi K, Ohsugi M, Hirano T (2017). Mitotic chromosome assembly despite nucleosome depletion in Xenopus egg extracts. Science 356, 1284–1287.
Shintomi K, Takahashi TS, Hirano T (2015). Reconstitution of mitotic chromatids with a minimum set of purified factors. Nat Cell Biol 17, 1014–1023.
Spence JM, Phua HH, Mills W, Carpenter AJ, Porter AC, Farr CJ (2007). Depletion of topoisomerase IIalpha leads to shortening of the metaphase interkinetochore distance and abnormal persistence of PICH-coated anaphase threads. J Cell Sci 120, 3952–3964.
Strom AR, Emelyanov AV, Mir M, Fyodorov DV, Darzacq X, Karpen GH (2017). Phase separation drives heterochromatin domain formation. Nature 547, 241–245.
Sullivan BA, Karpen GH (2004). Centromeric chromatin exhibits a histone modification pattern that is distinct from both euchromatin and heterochromatin. Nat Struct Mol Biol 11, 1076–1083.
Thadani R, Uhlmann F, Heeger S (2012). Condensin, chromatin crossbarring and chromosome condensation. Curr Biol 22, R1012–1021.
Tokunaga K, Saitoh N, Goldberg IG, Sakamoto C, Yasuda Y, Yoshida Y, Yamanaka S, Nakao M (2014). Computational image analysis of colony and nuclear morphology to evaluate human induced pluripotent stem cells. Sci Rep 4, 6996.
Yoshimura SH, Hirano T (2016). HEAT repeats—versatile arrays of amphiphilic helices working in crowded environments? J Cell Sci 129, 3963–3970.